Numerical Study of CO_2 monitoring using Time-lapse Down-hole Magnetometric Resistivity at Field Research Station, Alberta, Canada

*Abderrezak Bouchedda and Bernard Giroux *, INRS-ETE*

MMR Method

The MMR method is based on the measurement of low-level and low frequency magnetic fields associated to noninductive current flow through the ground (Figure 1).

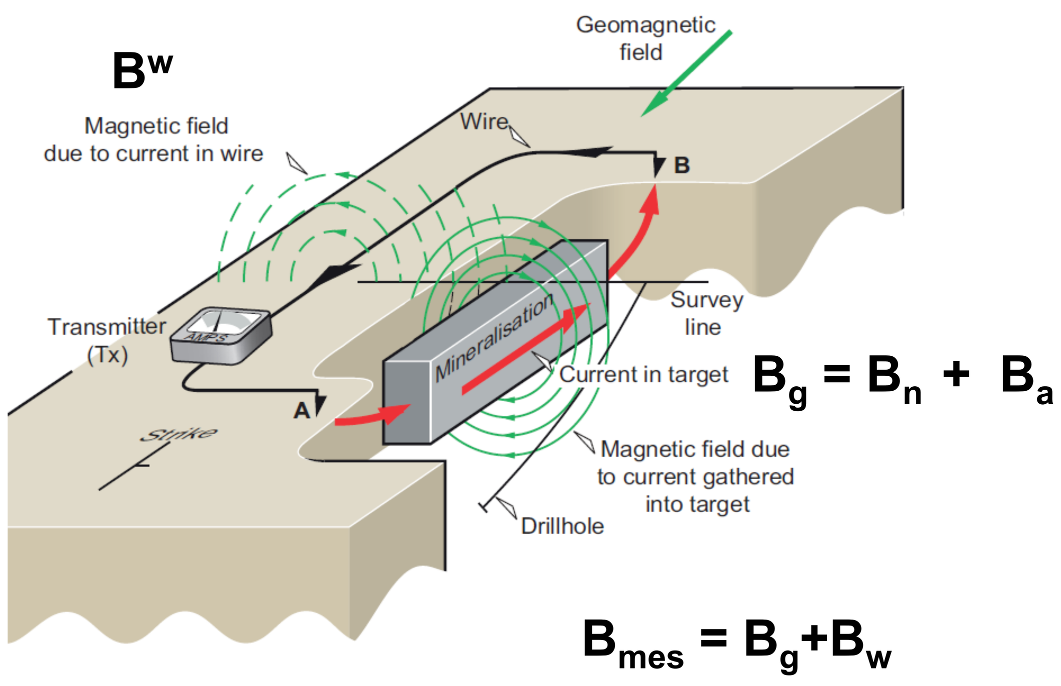

Figure 1: MMR method (after Denith et Mudge, 2014)

	MMR	DC resistivity	EM
Physical property	relative conductivity	conductivity	conductivity
Anomaly	currents channeling (Current density)	discontinuity of $\mathbf{E}_n$ (Current flows)	Secondary magnetic field (Induction)
Difficulties	-Receiver orientation. -EM noises. - Not sensitive to structures ⊥ to currents flow direction	-Bad electrode contacts. -Weak potential in highly conductive medium. -small size heterogeneities near the receiver greatly affect the measurements.	-Receiver orientation. -EM noises.
Small size structure near the receiver	Sensitive but the struct. can be masked (volume effect).	depends on electrodes separation.	Not sensitive
Weak conductivity contrast	Sensitive	Sensitive	Not sensitive
Conductive overburden	depth of investigation better	depth of investigation good	depth of investigation poor

MMR forward modeling equations using finite-volumes (Chen et al., 2002)

$$\nabla_h \cdot \mathbf{S}\nabla_h\phi = \nabla_h \cdot \mathbf{J}^s,$$

DC resistivity equation (Pidlisecky et al. 2007)

and

$$\left(\nabla_h^{(e)} \times \mathbf{M}_e^{-1}\nabla_h^{(f)} \times -\nabla_h \mathbf{M}_c^{-1}\nabla_h\cdot\right)\mathbf{A} = \mathbf{J}^s - \mathbf{S}\nabla_h\phi.$$

Magnetostatic equation

$\nabla_h^{(e)}\times$ $\nabla_h^{(f)}\times$: the curl operators, projecting from cell edges to faces and from faces to edges, respectively.

$\nabla_h \cdot$ *and* ∇_h *:* the divergence and gradient operators.

S : Matrix of harmonic averaging of the conductivity at the cell centres

$\mathbf{M}_e$ and $\mathbf{M}_c$ **:** Matrix of arithmetic averaging of the permeability at cell edges and the permeability at the cell centres

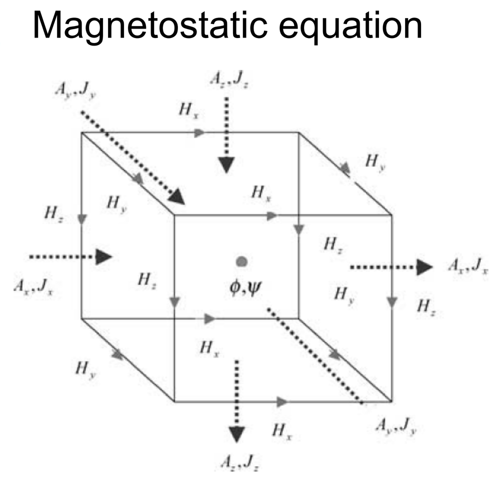

Discretization using finite Volumes (after Chen et al., 2002)

MMR time-lapse inversion

Consider a monitoring experiment where $\mathbf{d}_0$ and $\mathbf{d}_1$ are the MMR survey data acquired before and some time after CO_2 injection respectively. The difference inversion algorithm (Labrecque and Yang, 2001) consists in minimizing the misfit between the difference in two datasets and the difference between two corresponding model responses. The objective function to minimize is

$$\phi(\mathbf{m}) = \left\|\mathbf{W}_d(\Delta\mathbf{D})\right\|_2^2 + \beta\left\|\mathbf{C}\cdot(\Delta\mathbf{m})\right\|_2^2.$$

where $\mathbf{\Delta D} = (\boldsymbol{F}(\mathbf{m}) - \boldsymbol{F}(\mathbf{m}_0)) - (\mathbf{d}_1 - \mathbf{d}_0)$, $\mathbf{\Delta m} = \mathbf{m} - \mathbf{m}_0$, with **m** being the logarithm of conductivity, and $\mathbf{m}_0$ the model obtained after inversion of the baseline data $\mathbf{d}_0$. Also, ***F*** is the forward model operator, $\mathbf{W}_d$ is the data-weighting matrix, and **C** is a regularization matrix.

The model parameters are weighted using a distance-base weighting function as defined by Li and Oldenburg (2000). It is independent of the sensitivity calculation and is not affected by the directional variation.

Field Research Station site

The Field Research Station (FRS) is located in the South-East of Calgary in Newell county near Brooks town (Figure 2), Alberta, Canada. It is under development and consists of 1 x 1 km² flat area. The first injection well is 500 m deep and was drilled in February 2015. Figure 2 shows the FRS infrastructures as will be constructed by Schlumberger Carbon Services before the end of 2015.

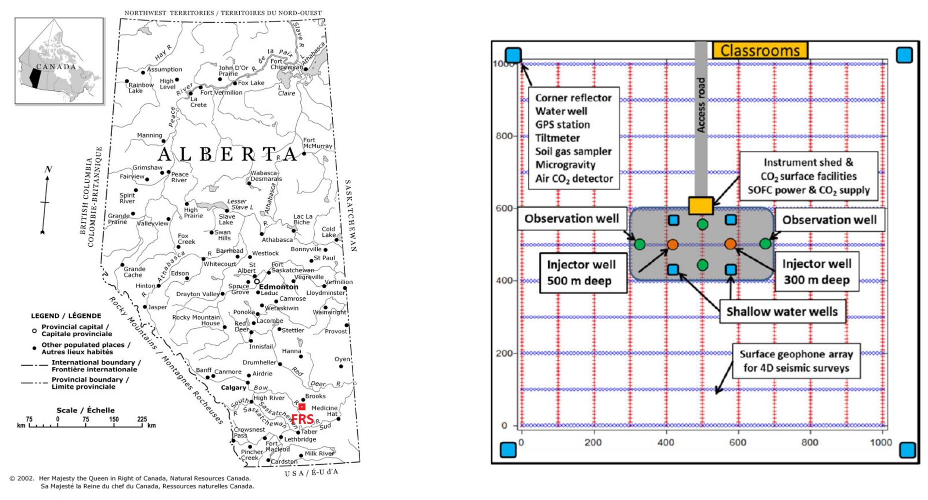

Figure 2: Location and schematic Field Research Station layout.

3-D seismic shows that geology at the FRS site is mostly 1D. To build the resistivity model of FRS that served to generate the synthetic data, we used a smoothed version of the resistivity well log data shown in Figure 3.

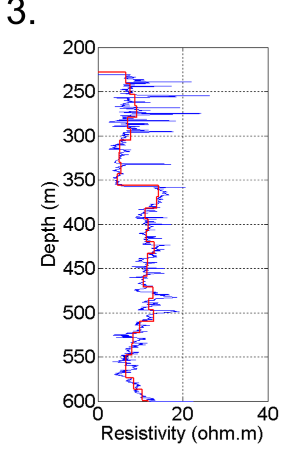

Figure 3: Resistivity well log at FRS (blue line) and resistivity model obtained by Haar wavelet approximation of resistivity well logs (red line).

Numerical tests

For the numerical experiments, a model of size 350×350×350 m³ was discretized using a mesh with 12.5×12.5×10 m³ voxels. Between 230 m and 320 m depths, the step size in the vertical direction was decreased to 5 m. The MMR data were generated by considering two transmitter configurations corresponding to two electrodes orientations that are perpendicular each other.

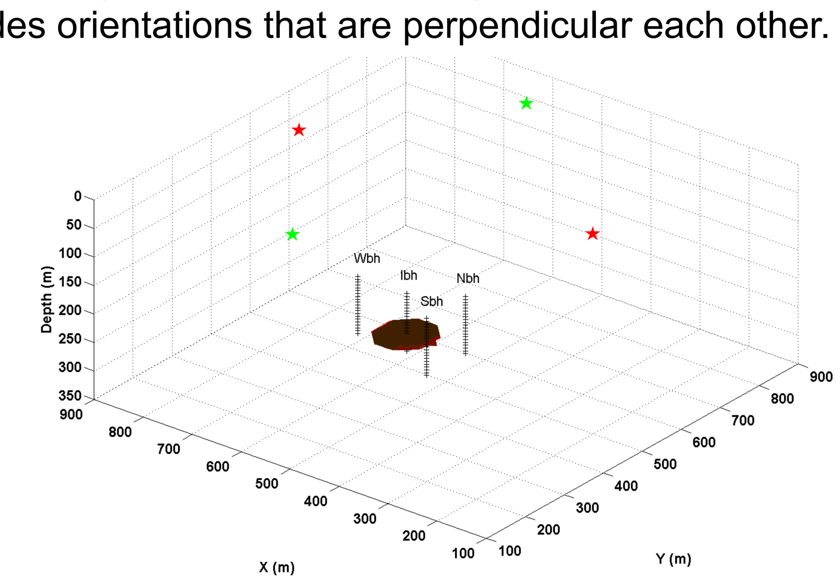

Figure 4: MMR measurements setup and CO_2 plume location (red disc). Green and red stars correspond to first and second electrodes configuration respectively.

The injection target is located between 290 m and 295 m depths and has a resistivity of 7 ohm.m. The CO_2 plume is modeled as a resistive disc of 10 times the resistivity of sandstone. The thickness of the disc was fixed for all experiments to 5 m and its center is at a depth of 297.5 m. To simulate the evolution of the CO_2 plume, two scenarios were considered. At each time lapse, the radius of the plume is increased from 50 m (time t_1) to 100 m (time t_2). The MMR measurements are performed in 4 boreholes at 5 m step between 220 m and 320 m depth

Qualitative interpretation

Figure 5 shows the magnetic field response difference between observed magnetic fields before and after CO_2 injection at Wbh (680,500). For the 50 m radius plume, it is not possible to detect its effect because the magnetic field difference appears as a weak long-wavelength anomaly. When the plume radius increases to 100 m, its effect is clearly observable in the data. This can be explained by the fact that MMR anomaly is caused by resistivity contrasts and is inversely proportional to the distance between the receivers and the resistivity contrasts.

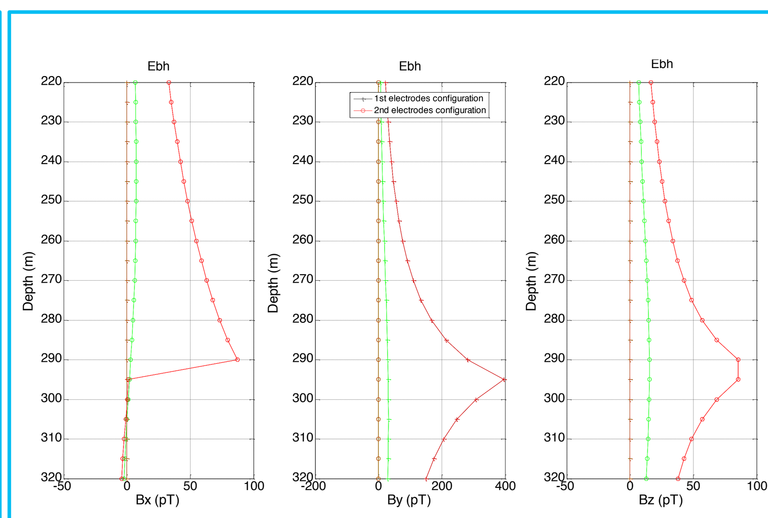

Figure 5: MMR field difference at time-lapses t_1 and t_2 for the two electrodes configuration. Green line corresponds to time-lapse t_1 and red line corresponds to time-lapse t_2.

Time-Lapse inversion results

To follow the evolution of the plume, time-lapse inversions were carried out using observed MMR data at time intervals t_1-t_0 and t_2-t_0.

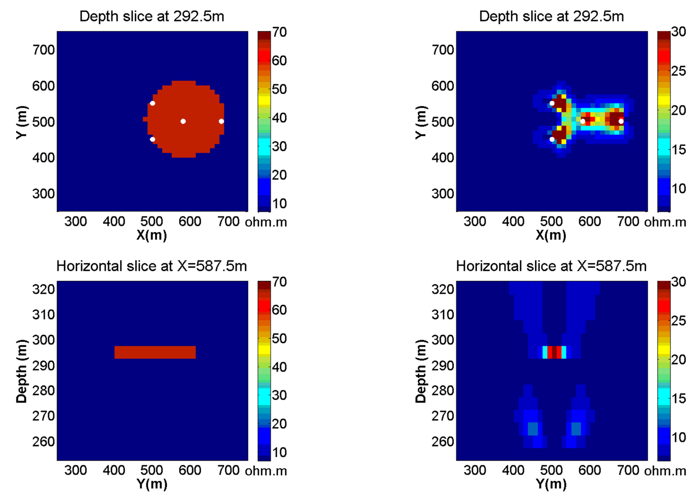

Figure 6: Left: real resistivity model; Right: resistivity model obtained by time-lapse inversion t_2-t_0. White dots show the location of the borehole measurements.

Inversion results for t_2-t_0 without using model weighting function are shown in Figure 6. The depth of the CO_2 plume is well retrieved but the lateral extensions are not well resolved. The resistive plume tends to be elongated in the same direction as the current electrodes orientation and is concentrated around borehole observation. This can be explained by the fact that there is a bias towards channelling currents along structures with a similar orientation to the current electrodes and to geometric decay of the response with distance, similar to what can be observed in gravity (Chen et al., 2002).

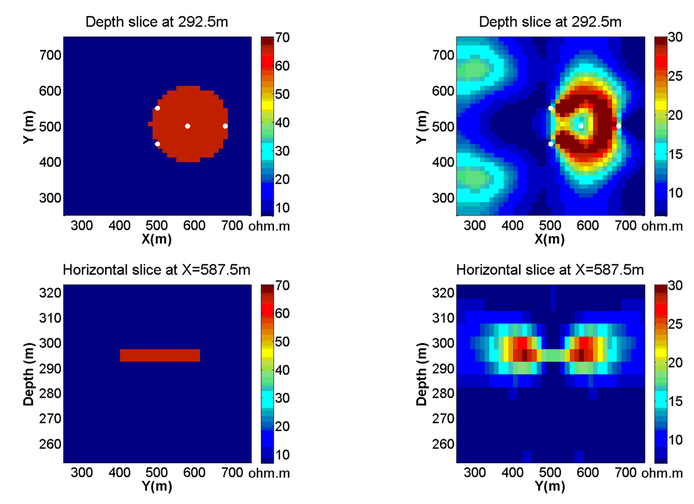

Figure 7: Left: real resistivity model; Right: resistivity model obtained by time-lapse inversion t_0-t_2 using weighting function. White dots are borehole measurements.

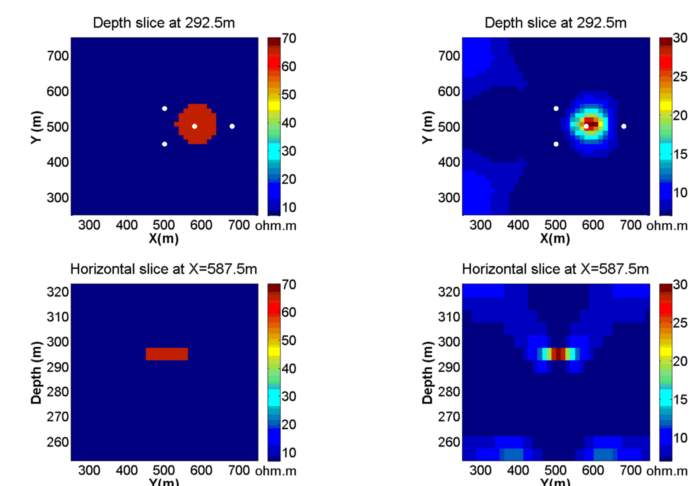

Figure 8: Left: real resistivity model; Right: resistivity model obtained by time-lapse inversion t_0-t_1 using weighting function. White dots are borehole measurements.

When the model weighting function is included in the inversion, the lateral extensions of the plume are more realistic. However, the circular region around Ibh appears less resistive (Figure 7). This is due to the combination of weak MMR response at Ibh (resistivity contrasts are 100m far from Ibh) and to the desensitization of resistivity blocks caused by weighting model function around Ibh.

Acknowledgments

This work was supported by Carbon Management Canada, CMC-NCE, grant C394 to B. Giroux. The authors would like to thank Don Lawton for providing the FRS well logs data.

References

-Chen, J., Haber, E., and Oldenburg, D.W. [2002] Three-dimensional numerical modelling and inversion of magnetometric resistivity data. *Geophysical Journal International*, **149**, 679-697.

-Denith, M. and Mudge, S. T. [2014] Geophysics for the mineral exploration geoscientist. Cambridge University Press.

-Edwards R.N. [1974] The magnetometric resistivity method and its application to the mapping of a fault. Canadian Journal of Earth Sciences, **11**, 1136–1156.

-Pidlisecky, A.; Haber, E. & Knight, R. [2007] RESINVM3D: A 3D resistivity inversion package. Geophysics, **72** , H1-H10.

-LaBrecque, D., and X. Yang, 2001, Difference inversion of ERT data: a fast inversion method for 3-D in situ monitoring: Journal of Environmental and Engineering Geo-physics, 6, 83–89.

- Li, Y. and Oldenburg, D. W., 2000, Joint inversion of surface and three-component borehole magnetic data, Geophysics, **65**, 540-552.